Available online at www.sciencedirect.com
ScienceDirect
Journal of Photochemistry and Photobiology A: Chemistry 187 (2007) 299–304
Journal of Photochemistry and Photobiology A:Chemistry
www.elsevier.com/locate/jphotochem

Time-resolved photoluminescence of terbium-doped microporous–mesoporous Zeotile-1 materials

C. Tiseanu [a,*], M.U. Kumke [b], V.I. Parvulescu [c], A.S.R. Koti [d], B.C. Gagea [e], J.A. Martens [e]

[a] National Institute for Laser, Plasma and Radiation Physics, P.O. Box MG-36, RO 76900, Bucharest-Magurele, Romania
[b] Institute of Chemistry, Physical Chemistry, University of Potsdam, Karl-Liebknecht-Str. 24-25, 14476 Potsdam-Golm, Germany
[c] University of Bucharest, Department of Chemical Technology and Catalysis, 4-12 Regina Elisabeta Bvd., Bucharest 030016, Romania
[d] Department of Biological Sciences, Columbia University, New York, NY, United States
[e] Department of Interphase Chemistry, KU Leuven, 23 Kasteelpark Arenberg, B-3001 Leuven (Heverlee), Belgium

Received 2 July 2006; received in revised form 24 October 2006; accepted 26 October 2006
Available online 3 November 2006

Abstract

Time-resolved luminescence spectra and decays were analyzed for the as-synthesized (hydrated) as well as for the calcined terbium-exchanged microprous–mesoporous Zeotile-1 materials. On the basis of photoluminescence decays, peak and area normalized time-resolved photoluminescence spectra, one species for the hydrated terbium–Zeotile-1 and two species for the calcined terbium–Zeotile-1 materials were evidenced, respectively. Our results highlighted that combined information from both spectral- and time-domain could bring more reliable information on the lanthanide distribution in these highly heterogeneous materials.

Keywords: Time-resolved pholuminescence; Zeolites; Spectral lineshapes; Lanthanide ions

1. Introduction

Zeolites are microporous materials which found many and very interesting applications [1]. Although they exhibit large surface areas, these applications are limited to small molecules, since molecules with kinetic diameter higher than 8 Å can hardly penetrate inside the micropores. The use of the mesoporous materials was reported to overcome these problems [2]. However, although mesoporous materials offer great advantages in term of diffusion properties, many of the chemical and physical applications are limited by the lack of atomic order in the pore walls. A recent alternative to this problem is represented by the hierarchical materials [3–7]. These porous materials with two or more levels of porosities have already attracted much attention owing to their potential applications in catalysis, separation, ion-exchange, and as sensitive chemosensing films [8]. Such materials improve the diffusion of the guest molecules through the inorganic network of pores and channels, because larger pores allow for better molecular accessibility while the smaller pores provide high surface areas and large pore volumes. Already many solutions have been proposed for synthesis of the hierarchical materials [9]. Another approach in preparation of mesoporous materials with crystalline walls was proposed by Martens. Accordingly, a family of such mesoporous materials, Zeotile-1 (ZT1) can be synthesized by stapling together, with the help of secondary templates, MFI precursor units (nanoslabs) [10,11]. Most of the applications of the zeolite-type materials are related either to the acid properties of the OH groups or on the location and aggregation of the exchanged metal species. Therefore, it is extremely important to know both the location and coordination of these species. Lanthanides (Ln^{3+}) doped porous materials have attracted a great interest in the last years due to their potential application in luminescent and laser materials, polarizers, for second harmonics generation, optical switching, data storage and phosphors [12–16]. There are also many references about the use of various lanthanides as photoluminescence (PL) probes for zeolites structures, especially faujasites. However, compared to faujasites, the distribution and coordination of lanthanides in MFI zeolites such as ZSM-5 is poorly understood. In previous studies involving the time-resolved photoluminescence characterization of Eu^{3+}-doped ZSM-5, it was found out that the coordination number in ZSM-5 is smaller than that in

* Corresponding author. Fax: +40 1 423 17 91.
E-mail address: tiseanuc@yahoo.com (C. Tiseanu).

1010-6030/$ – see front matter © 2006 Elsevier B.V. All rights reserved.
doi:10.1016/j.jphotochem.2006.10.026

Table 1
Characteristics of Tb–Zeotile-1 materials

No.	Notation	System	Si/Al ratio	Tb content (wt.%)	BET surface (m^2/g)	Pore size (nm)
1	Tb–ZT1(33)	Tb-zeolite MFI-hexagonal structure	33	1.05	962	2.2
5	Tb–ZT1(100)	Tb-zeolite MFI-hexagonal structure	100	0.49	1176	2.5
7	Tb–ZT1(200)	Tb-zeolite MFI-hexagonal structure	200	0.34	992	2.5

water, which is due to the displacement of water from the Eu^{3+} by the framework oxygens [17]. Information related to Ce^{3+} or La^{3+} location was also collected from the intrazeolitic redox process of Ce^{3+}–Ce^{4+} in ZSM-5 [18] or from FT-IR studies [19]. Density functional calculations determined that lanthanum ions are favorably accommodated in the two 6-T rings of the straight channels of ZSM-5 [20] where they coordinate to six oxygen atoms, four of the oxygen atoms come from the zeolite framework while the other two come from the hydrolysis of lanthanide hydrate.

In this report, we present the phophysical characterization of the hybrid microporous–mesoporous Zeolites doped with lanthanide ions such as terbium (Tb^{3+}). The analysis on the time-resolved photoluminescence spectra and luminescence decays allowed us to estimate the nature of the lanthanides distribution in these materials, such as single *versus* multiple species in the hydrated and calcined states.

2. Experimental section

2.1. Synthesis

Nanoslabs with MFI structure type are prepared through hydrolysis of tetraethylorthosilicate (TEOS) in concentrated solution of tetrapropylammonium hydroxide (TPAOH) [21]. Aluminum containing nanoslabs were prepared by first dissolving the appropriate amount of Al metal powder in TPAOH 40 wt.% followed by addition of TEOS and water using the procedure for all silica nanoslabs. The final composition of the nanoslab clear solution was $Si_{(9-x)}$:$Al_{(x)}$:$TPAOH_{(25)}$:$H_2O_{(400)}$.

The aluminum containing nanoslabs were further used to prepare hybrid Zeotile-1 zeolites [11]. The nanoslab suspension was mixed with 10 wt.% aqueous CTABr solution at 80 °C under stirring. The precipitate was then separated by filtration, washed, dried at 60 °C for 12 h and calcined at 550 °C for 5 h using a heating rate of 1 °C/min. The materials were subjected to an ionic exchange treatment following a previously reported procedure [22]. Then 1 g of freshly material was added in 25 ml of 0.004 M Tb^{3+} aqueous solution and stirred for 30 min at 80 °C. The samples were then recuperated and dried in an air oven at 120 °C for 24 h. Calcination was pursued in air at 450 °C at a heating rate of 5 °C/min.

2.2. Characterization

Characterization of these materials was carried out using adsorption–desorption isotherms of nitrogen at 77 K, and XRD. Sorption isotherms of N_2 were obtained with a Micromeritics ASAP 2000 apparatus after outgassing the samples at 423 K for 12 h under vacuum. The XRD patterns were obtained with a SIEMENS D-5000 diffractometer at 40 kV and 50 mA, equipped with a variable-slit diffracted-beam monochromator and scintillation counter. The diffraction patterns were recorded in the range 0–80° 2θ using Cu Kα radiation (λ = 1.54183 Å). The N_2 adsorption isotherm of Tb–ZT1 samples show a hysteresis loop characteristic to mesoporous materials with the mean pore size of 2.2–2.5 nm (BJH method) and a BET surface area of around 1000 m^2/g. Notation for Zeotile materials, Si/Al ratio, Tb^{3+} concentration (determined by ICP-AES) together with the textural results are gathered in Table 1. As terbium is found only as trivalent ion, "Tb" notation was also used throughout the paper.

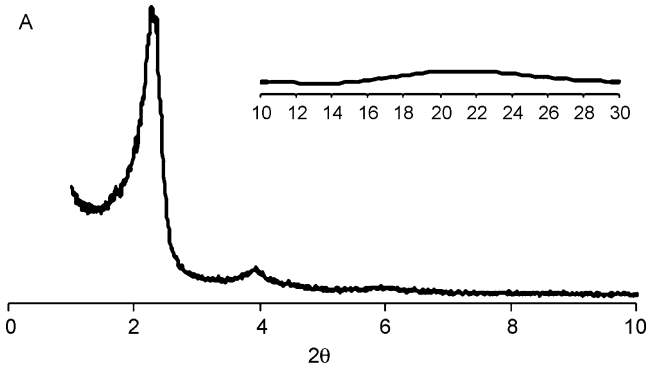

Fig. 1. XRD-patterns of terbium–ZT1(3 3).

Fig. 1 shows the XRD patterns of the investigated samples where only the low angle peaks were evidenced. The absence of diffraction lines at higher 2θ angles proves that the ZT1 materials are build from zeolite precursor units and that there are no big MFI domains present.

2.3. Photoluminescence measurements and analysis

The stationary luminescence measurements were carried out at 20 °C using a Fluoromax 3 spectrofluorometer (Jobin Yvon). The instrument was operated in the phosphorescence mode, with excitation wavelengths chosen according to the laser wavelengths used in the time-resolved experiments. The repetition rate of the flash lamp was 25 Hz, the integration window 0.5 ms, the delay after flash was set to 0.1 ms, and 50 flashes were accumulated per data point. The slits were set to 2 nm spectral bandwidth in excitation as well as emission. In the time-resolved luminescence measurements, a nitrogen laser (LTB) operated at 10 Hz was employed. The luminescence was detected at a right-angle geometry in spectral range of 450 nm < λ_{em} < 650 nm using an intensified CCD camera (Andor DH720-18H-13) equipped with a spectrograph (MS257, Oriel Instruments). The detection window was set to 10 μs, which

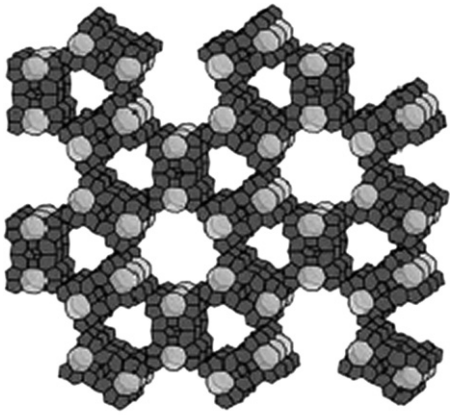

Scheme 1. Structure of Zeotile-1 materials. Nanoslabs with MFI structure are linked to form a pattern with hexagonal symmetry.

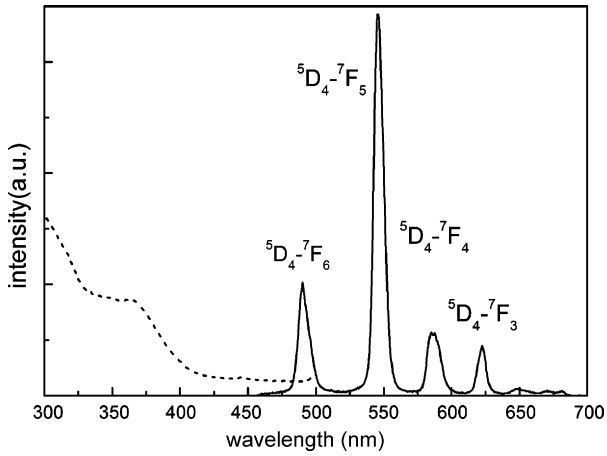

Fig. 2. Representative excitation (dotted line) and PL emission (solid line) spectra of hydrated terbium–ZT1 ($\lambda_{em} = 545$ nm, $\lambda_{ex} = 337$ nm).

was shifted in steps of 20 μs over a total time of 3.0 ms for the hydrated Tb-zeolites and in steps of 60–80 μs over a total time of 12–16 ms for the calcined Tb-zeolites. A typical acquisition time of a complete TRES experiment was about 20 min. The PL transients were deconvoluted using a multiexponential function: $f(t) = \sum_{i=1}^{n} A_i \exp(-t/\tau_i) + B$, where A_i is the decay amplitude, B the constant (the baseline offset) and τ_i is the decay time. The PL decays were also analyzed according to a lifetime distribution analysis with decay times equally spaced in $\ln(\tau)$ allowing for symmetric distributions as well as Voigt profiles (Gaussian and Lorentzian mixture). The full description of the method is given in [23]. The time resolved photoluminescence spectra (TRES) were further analyzed using peak normalization and area normalization (TRANES) to understand the heterogeneity associated with the system. The TRANES were constructed by normalizing the area of each spectrum in TRES such that the area of the spectrum at time t is equal to the area of the spectrum at $t = 4$ μs [24–26].

3. Results and discussion

Scheme 1 depicts the structure of Zeotile-1-type materials. Due to the synthesis conditions the nanoslabs aggregated in a hexagonal structure around the CTABr micelles (Scheme 1) [10]. In addition to micropores, this material contains mesopores of 2.2–2.5 nm (Table 1). Terbium is located in these materials on both internal and external surface areas in a close proximity of aluminum centers. The loading of terbium ions parallels the concentration of the aluminum exchange species (Table 1).

3.1. Photoluminescence of hydrated Tb–Zeotile-1

Illustrated in Fig. 2 are the representative photoluminescence and excitation spectra of the hydrated Tb–ZT1 zeolites.

Terbium PL spectrum displays the $^5D_4$–$^7F_3$, $^7F_4$, $^7F_5$, $^7F_6$ transitions spanning from 450 nm < λ_{em} < 650 nm. The most intense PL band located at 545 nm was used in the PL decays measurements and TRES spectra analysis. Fig. 3 shows the differences observed with spectral-shapes and decays of terbium 545 based PL in Zeotile-1 with different Si/Al ratio.

The FWHM values slightly increase with Si/Al ratio and even a fine structuring of terbium PL in Zeotile-1 with highest Si/Al ratio (2 0 0) is observed.

The PL decays measured at 545 nm are non-exponential in all samples (Fig. 3, inset). A non-exponential shape of luminescence decays can be generally explained in terms of Zeotile-1 framework heterogeneity, where terbium ions can occupy different sites or/and due to the presence of non-radiative energy transfer processes. Terbium lifetime τ related to the PL emission from the metastable $^5D_4$ state is described as:

$$\tau = \frac{1}{(k_r + k_{nr} + k_{nr^*})} \quad (1)$$

where k_r is the natural radiative rate constant, k_{nr} the rate constant for the non-radiative relaxation processes due to –OH coupling and k_{nr^*} is the rate constant for the radiationless relaxation processes due to other processes than –OH coupling. The radiationless deactivation processes due to –OH coupling is a well-known contribution to the alteration of the PL quantum

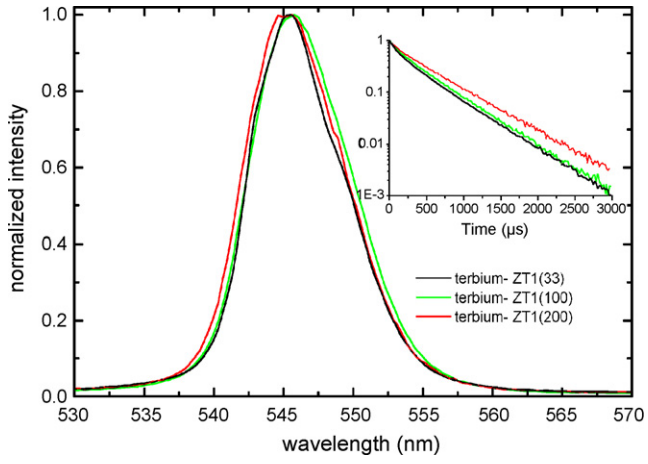

Fig. 3. Comparison between PL spectra of hydrated Tb–ZT1 in the range 530 nm < λ_{em} < 560 nm. Inset: PL decays of hydrated Tb–ZT1.

Table 2
PL decay parameters of Tb–Zeotile-1 materials

Sample	Hydration state	Decay times τ_i (μs) and amplitudes A_i (%) in brackets			χ^2
Tb–ZT1(3 3)	Hydrated	180(37)		474(63)	0.99999
	Calcined	355(24)	1043(64)	2195(12)	0.9996
Tb–ZT1(1 0 0)	Hydrated	183(34)		518(66)	0.99999
	Calcined	314(13)	860(70)	1906(17)	0.9995
Tb–ZT1(2 0 0)	Hydrated	184(18)		535(82)	0.99999
	Calcined	325(24)	976(57)	1996(19)	0.9995

efficiency of lanthanides in sol–gel materials. Zeolite framework exhibits only low energy phonons, which are not expected to contribute to the non-radiative deactivation of Tb photoluminescence [12]. PL quenching may be also related to ion–ion interactions located in close proximity, generally negligible for the $^5D_4$ level and at the concentrations used [27], or/and non-radiative energy transfer to surface defects or impurities. Further studies are needed to elucidate whether such quenching processes manifest in Zeotile-1. The non-exponential PL decays of hydrated terbium–Zeotile-1 were satisfactory fitted to a bi-exponential function which evidenced besides a short, relatively constant decay time at about 180 μs a longer decay time whose values increase with Si/Al ratio from 470 μs in ZT1(3 3) to 535 μs in ZT1(2 0 0), Table 2.

Generally, a two terbium species suggested by the discrete exponential analysis of PL decays may be further validated through site selective excitation spectra or/and time-resolved PL spectra. Due to the broadness nature of the excitation spectra of Tb–ZT1 (Fig. 2), the time-resolved photoluminescence spectra (TRES) were used instead as an indicative of the system heterogeneity [28]. It was found that, while the time-resolved photoluminescence spectra of terbium–ZT1 evolved continuously in the time range of 4 μs < t < 3000 μs after laser excitation pulse, no differences in peak positions, spectral line width and spectral shape were found in the peak-normalized TRES (Fig. 4). Therefore, it is reasonable to conclude that, in the hydrated Zeotile-1, terbium is found as single species with lifetime varying between 450 and 570 μs according to the Si/Al ratio (Table 2).

The dependence of the luminescence intensity, decay as well as the spectral lineshape on the Si/Al ratio suggest that the interaction of terbium ions with ZT1 is sizeable even for the hydrated samples, where the water molecules are expected to shield terbium ions against matrix effects (Fig. 3). As in water, Tb shows monoexponential luminescence decay kinetic with a luminescence decay time of 395 ± 10 μs, the values listed in Table 1 sustain a mixed contribution of water molecules and framework oxygens to terbium coordination in Zeotile-1. Terbium is expected to occupy a position in the close proximity of aluminum with the involvement of a single interaction with the network, although an additional interaction with a second aluminum network, or deposition nearby a silicon are not excluded [29]. For the hybrid microporous–mesoporous Zeotile-1 the dominant surface is the external one (Table 1). Under these conditions, Tb would prefer the sites located on the external wall of Zeotile-1 to those in channels, which require additional mass transfer limitations to be reached.

3.2. Photoluminescence of calcined Tb–Zeotile-1

Upon calcining in air at 450 °C, the terbium PL is broadened (Fig. 5), with stronger intensity as well as longer decays compared to those measured for the hydrated samples (Fig. 5, inset).

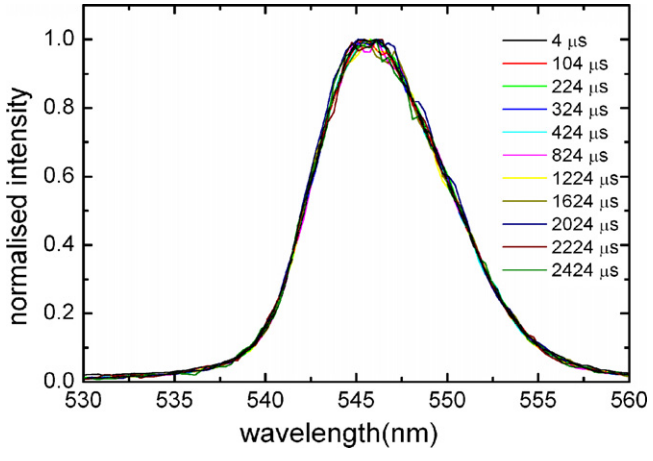

Fig. 4. Peak normalized time-resolved luminescence spectra of hydrated terbium–ZT1(2 0 0). All curves represent experimental data.

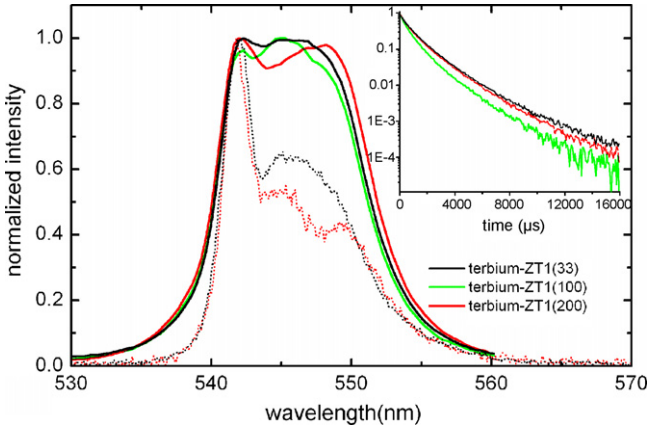

Fig. 5. Comparison between the PL spectra of calcined Tb–ZT1 in the range of 530 nm < λ_{em} < 560 nm. With dotted lines are represented the PL spectra of calcined Tb–ZT1(3 3) and Tb–ZT1(2 0 0) at 80 K. Inset: PL decays of the calcined Tb–ZT1.

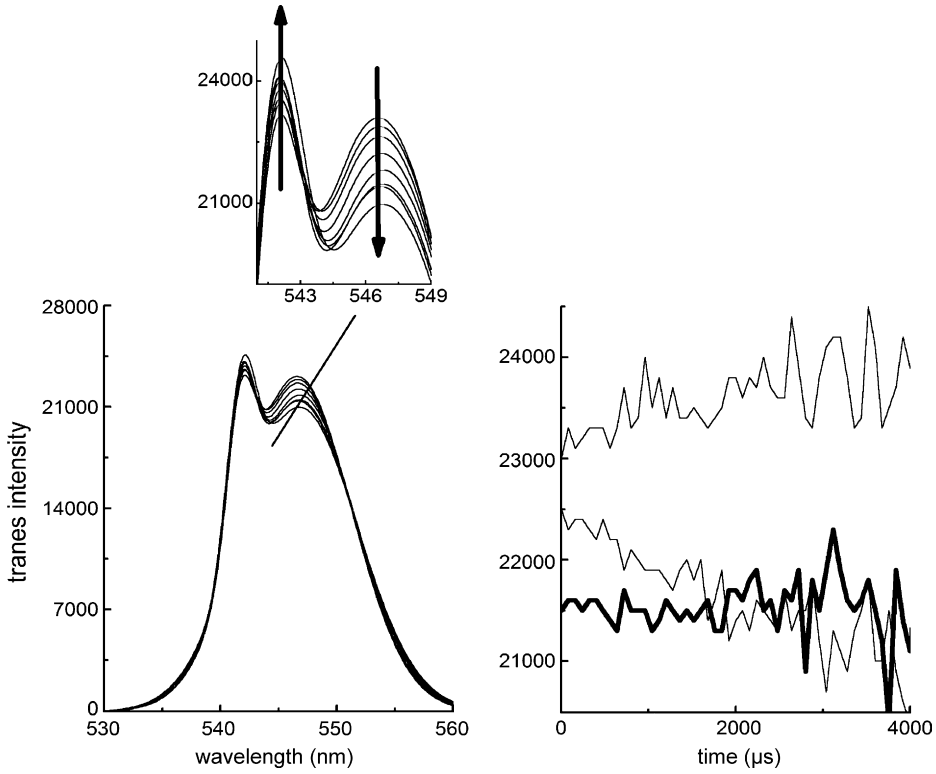

Fig. 6. Isoemissive emissive point in the TRANES spectra of calcined Tb–ZT1(2 0 0) confirms the presence of two species. Left: TRANES spectra in the time range 4–4000 μs. The intensity profiles are smoothed by using two log–normal functions. Inset shows the peak region of the TRANES spectra in detail. The arrows indicate the time from 4 to 4000 μs. Right: time dependency of the TRANES intensity measured at the isoemissve point, 543 nm (thick-line) and at two emission wavelengths which display maximum increase (at 542 nm) and maximum decrease (at 548.2 nm) of the intensity with time (thin lines). These curves represent the experimental data.

The framework modification at the terbium sites upon calcining is evidenced by the broadening of the PL spectra (FWHM values increase from 7 to 9 nm in the hydrated samples to more than 13 nm in the calcined samples) as well as the occurrence of a fine structuring. At least three exponentials were needed in the decay analysis (Table 2). The decay times vary between 310 and 360 μs, 860 and 1043 μs and 1906 and 2195 μs with the median decay times accounting for more than 50% of the total decay amplitude.

For the hydrated terbium–ZT1, a mixed coordination of ion to both water and framework oxygen's was found, with the first contribution as dominant. Upon calcining, the coordination of terbium ions changes as water is removed form the first coordination sphere.

The framework modifies to accommodate the new coordination requirements of the terbium ions or they can migrate to a different position where they can obtain a higher coordination environment [30]. With increasing the Si/Al ratio, it is expected however, that terbium migration insight the channels even in the presence of water would become more difficult. Once entrapped in the position where the channels are interpenetrated, terbium coordination with water will be limited by the interactions with the network.

The three species model in the calcined terbium–ZT1 as suggested by fitting results of the PL decays was also probed by TRES analysis. In contrast to the hydrated samples, the peak-normalized TRES spectra of the calcined zeolites display a continuous variation in the time range of $4\,\mu s < t < 16{,}000\,\mu s$ after laser excitation pulse: for example, for terbium ZT1(2 0 0) the peak-normalized TRES spectra at 542 nm, evidence a continuous decrease of the PL intensity of the 548.2 nm centered peak. Therefore, more than one terbium species is expected in the calcined Zeotile-1. To specify the number of terbium species, which is responsible for the observed TRES behaviour is not straightforward. A new model-free analytical method called the time resolved area normalized emission spectroscopy (TRANES) was successfully applied to study the heterogeneity of probe distribution in bilayer membranes [24–26]. Compared to TRES, TRANES has a physical significance: An isoemissive point in TRANES occurs at the wavelength (λ_{iso}) where the ratio of the wavelength-dependent radiative rates ($k_{r1}(\lambda_{iso})/k_{r2}(\lambda_{iso})$) is equal to the ratio of the total radiative rates (k_{r1}/k_{r2}) of the emitting species.

$$\frac{k_{r1}(\lambda_{iso})}{k_{r2}(\lambda_{iso})} = \frac{k_{r1}}{k_{r2}} \tag{2}$$

Here, we apply TRANES analysis to investigate the heterogeneity of the calcined terbium-doped ZT1 materials. Fig. 6 shows the TRANES spectra of the Tb–ZT1(2 0 0). In these TRANES spectra, an isoemissive point at 543 ± 3 nm is observed, where the intensity is constant and does not change with time. This is clearly demonstrated in Fig. 6 (left), where the intensity at the isoemissive point is time independent. In addition, we also show the intensities at two other wavelengths on

either side to the isoemissive point, which display a maximum increase (at 542 nm) or decrease (at 548.2 nm) of intensity in the measured time interval.

This further supports the presence of the isoemissive point at 543 ± 0.3 nm for Tb–ZT1(2 0 0). For the Tb–ZT1(1 0 0) and ZT1(3 3) samples, TRANES analysis provides similar results with some differences between the positions of isoemissive points. This is an expected result as the Si/Al variation induced different crystal-fields at the Tb sites, which in turn determined slightly different spectral properties. Such an effect is more evident at 80 K (Fig. 5). More, the small dependency of FWHM on temperature confirms that the broadening mechanism of terbium PL in Zeotile-1 is primary inhomogeneous, arising from the increased heterogeneity of the ion environment upon calcination.

On the basis of the various reports on the broad lifetime distributions of excited states of guest molecules in zeolites [23,31], in-going studies carefully assess a similar approach for the lanthanides. A distribution of environments or sites whether these are located on the surface or inside channels is sustained by the highly heterogeneous nature of zeolites structure. Preliminary results on PL decay analysis using a mixture of Gaussian and Lorentzian distributions as described in [23] show, besides a small (less than 10%) narrow amplitude short decay at about 60 μs, two overlapped lifetimes distributions centered on 600–1000 μs and 1600–2000 μs, respectively. Such a lifetimes distribution analysis is also validated by the more sophisticated Maximum Entropy Method-based analysis of the time-resolved luminescence properties of lanthanides in microporous/mesoporous materials (C.Tiseanu et al., to be submitted). According to the above results, a two-terbium species with lifetime distributions instead of three discrete components is more realistic for the calcined terbium–Zeotile-1. Terbium location may be assigned to the internal surface (shorter lifetime species) or to more buried sites (longer lifetime species) within ZT1 framework.

4. Conclusions

A first investigation on the distribution of lanthanides in hybrid microporous–mesoporous Zeotile-1 materials was pursued by means of photoluminescence decays and time-resolved luminescence spectra. In contrast with the discrete exponential fit, analysis of the time-resolved luminescence spectra sustained a single terbium species coordinated to both water molecules and framework oxygens in the hydrated terbium–Zeotile-1 materials. For the calcined terbium–Zeotile-1, the interpretation of data is more complex. On the basis of the discrete exponential fit, lifetimes distribution analysis, peak and area normalized time-resolved photoluminescence spectra a two species distribution of terbium ions is proposed. Our study highlights the need for caution when interpreting non-exponential decays of lanthanides in mesoporous or zeolite materials in terms of a discrete number of emissive species. In this respect, combined information from spectral- and time-domain can bring more reliable information concerning distribution of lanthanides in these highly heterogeneous materials.

References

[1] H. van Bekkum, E.M. Flanigen, P.A. Jacobs, J.C. Jansen (Eds.), Introduction to Zeolite Science and Practice, 2nd ed., Elsevier Science, Amsterdam, 2001.
[2] C.T. Kresge, M.E. Leonowicz, W.J. Roth, J.C. Vartuli, J.S. Beck, Nature 359 (1992) 710.
[3] B.T. Holland, L. Abrams, A. Stein, J. Am. Chem. Soc. 121 (1999) 4308.
[4] G. Zhu, S. Qiu, F. Gao, D. Li, Y. Li, R. Wang, B. Gao, B. Li, Y. Guo, R. Xu, Z. Liu, O. Terasaki, J. Mater. Chem. 11 (2001) 1687.
[5] K.H. Sandhage, M.B. Dickerson, P.M. Huseman, M.A. Caranna, J.D. Clifton, T.A. Bull, T.J. Heibel, W.R. Overton, M.E.A. Schoenwaelder, Adv. Mater. 14 (2002) 429.
[6] X. Cai, G. Zhu, W. Zhang, H. Zhao, C. Wang, S. Qiu, Y. Wei, Eur. J. Inorg. Chem. 18 (2006) 3641.
[7] F. Xiao, L. Wang, C. Yin, K. Lin, Y. Di, J. Li, R. Xu, D. Su, R. Schlögl, T. Yokoi, T. Tatsumi, Angew. Chem. Int. Ed. 45 (2006) 3090.
[8] S. Tao, Z. Shi, G. Li, P. Li, Chem. Phys. Chem. 7 (2006) 1902.
[9] L. Huerta, C. Guillem, J. Lattore, A. Beltran, R. Martinez-Manez, M.D. Marcos, D. Beltran, P. Amoros, Solid State Sci. 8 (2006) 940.
[10] S.P.B. Kremer, C.E.A. Kirschhock, A. Aerts, K. Villani, J.A. Martens, O.I. Lebedev, G. van Tendeloo, Adv. Mater. 15 (2003) 1705.
[11] S.P.B. Kremer, C.E.A. Kirschhock, M. Tielen, F. Collignon, P.J. Grobet, P.A. Jacobs, J.A. Martens, Adv. Funct. Mater. 12 (2002) 286.
[12] H. Maas, A. Currao, G. Calzaferri, Angew. Chem. Int. Ed. 41 (2002) 2495.
[13] M. Bredol, U. Kynast, C. Ronda, Adv. Mater. 3 (1991) 361.
[14] T. Justel, D.U. Wiechert, C. Lau, D. Sendor, U. Kynast, Adv. Funct. Mater. 11 (2001) 105.
[15] J. Rocha, L.D. Carlos, Curr. Opin. Solid State Mater. Sci. 7 (2003) 199.
[16] M.H. Kostova, R.A.S. Ferreia, D. Ananias, L.D. Carlos, J. Rocha, J. Phys. Chem. B 110 (2006) 15312.
[17] G.D. Stucky, L. Iton, T. Morrison, G. Shenoy, S. Suib, R.P. Zerger, J. Mol. Catal. 27 (1984) 71.
[18] S.B. Hong, J. Phys. Chem. B 105 (2001) 11961.
[19] I. Othman, R.M. Mohamed, I.A. Ibrahim, M.M. Mohamed, Appl. Catal. A 299 (2006) 95.
[20] G. Yang, Y. Wang, D.H. Zhou, J.Q. Zhuang, X.C. Liu, X.W. Han, X.H. Bao, J. Chem. Phys. 119 (2003) 9765.
[21] C.E.A. Kirschhock, V. Buschmann, S. Kremer, R. Ravishankar, C.J.Y. Houssin, B.L. Mojet, R.A. van Santen, P.J. Grobet, P.A. Jacobs, J.A. Martens, Angew. Chem. Int. Ed. 40 (2001) 2637.
[22] O.A. Serra, E.J. Nassar, G. Zapparolli, I.L.V. Rosa, J. Alloys Compd. 225 (1995) 63.
[23] T.J.F. Branco, A.M.B. do Rego, I.F. Machado, L.F.V. Ferreira, Phys. Chem. B 109 (2005) 15958.
[24] A.S.R. Koti, N. Periasamy, Proc. Indian Acad. Sci. (Chem. Sci.) 113 (2001) 157.
[25] A.S.R. Koti, G. Krishnamoorthy, N. Periasamy, J. Fluoresc. 13 (2003) 95.
[26] A.S.R. Koti, N. Periasamy, J. Chem. Phys. 115 (2001) 7094.
[27] Y. Choi, K.S. Sohn, H.D. Park, S.Y. Choi, L. Mater. Res. 16 (2001) 881.
[28] J.R. Lakowicz, Principles of Fluorescence Spectrometry, Plenum Press, New York, 1983.
[29] V.I. Parvulescu, M.A. Centeno, P. Grange, B. Delmon, J. Catal. 191 (2000) 445.
[30] P. Norby, F.I. Poshni, A.F. Gualtieri, J.C. Hanson, C.P. Grey, J. Phys. Chem. B 102 (1998) 839.
[31] J.C. Scaiano, M. Kaila, S. Corrent, J. Phys. Chem. B 101 (1997) 8564.